Phys. Status Solidi A **206**, No. 6, 1117–1122 (2009) / **DOI** 10.1002/pssa.200824453

physica status solidi a
www.pss-a.com
applications and materials science

Editor's Choice

Manifestation of ripples in free-standing graphene in lattice images obtained in an aberration-corrected scanning transmission electron microscope

U. Bangert[*,1], M. H. Gass[2], A. L. Bleloch[2], R. R. Nair[1,3], and A. K. Geim[3]

[1] School of Materials, University of Manchester, Manchester, M13 9PL, UK
[2] SuperSTEM, STFC Daresbury Laboratory, Warrington, WA4 4AD, UK
[3] School of Physics and Astronomy, University of Manchester, M13 9PL, Manchester, UK

Received 4 November 2008, revised 6 February 2009, accepted 9 February 2009
Published online 2 April 2009

PACS 61.46.–w, 68.37.Ma

[*] Corresponding author: e-mail ursel.bangert@manchester.ac.uk, Phone: +44 (0)161 306 3587

The shape of ripples in free-standing graphene is derived from bond length distributions in high-angle annular-dark-field (Z-contrast) images, obtained in an aberration-corrected scanning transmission electron microscope (superSTEM). Local undulation patterns can readily be visualized by applying fast Fourier transform procedures to the lattice images, using a spatial frequency filter which passes the precise graphitic *a*-plane spacing. Using aberration-corrected STEM presents the unique opportunity to correlate atomic resolution imaging with the undulations. Values for projected bond lengths, and hence bond inclinations, can be obtained by adjusting the filter to the appropriate band pass. Ripples with amplitude ~0.5 nm and width ~5 nm were observed. Their patterns modify in repeated image scans, with prolonged scanning introducing vacancies. These, in conjunction with adatoms which are also revealed in Z-contrast, induce highly localized changes in the mechanical properties of graphene. Ripples in defected graphene remain dynamic, with changes occurring together with redistribution of defects.

1 Introduction The stability of extended two-dimensional (2D) structures has been the subject of a long-standing theoretical debate, with previous suggestions that 2D films embedded in three-dimensional 3D space are crinkled. It was then countered that crinkles can be suppressed by anharmonic coupling between bending and stretching modes, such that a 2D membrane can exist but will nevertheless exhibit height fluctuations [1–3]. The mechanical behavior of graphene, the first true 2D crystal [4, 5], can have profound impact on its extraordinary electronic properties [6]. Recent observations suggest that suspended graphene is not perfectly flat, but rather exhibits microscopic corrugations (ripples) which can be not only dynamic (that is, through flexural phonons) but also static [1, 7, 8]. In those observations, large-scale ripples (>15 nm) were visualized directly [9], whereas ripples on a nanoscopic scale (<15 nm) were only identified from the broadening of diffraction spots [7], which prevents static and dynamic bending from being distinguished. Furthermore, it was argued that scaffolds supporting graphene crystals, and contamination by adsorbed hydrocarbons, can either induce an external compression resulting in ripples especially on the large scale, or by films 'remembering' the initial non-flat configuration induced by a silicon oxide substrate used for sample preparation. In either instance, the observed ripples would not be intrinsic. The difficulty with directly imaging ripples in a transmission electron microscope arises from their small amplitude: the defocus, even with aberration-correction, is not precise enough to reliably detail changes in contrast which would arise from height differences less than a few nanometers, let alone one nanometer.

In the present contribution, a method of imaging ripples is discussed, which does not employ defocusing methods; in fact the atomic lattice is clearly visible throughout. High-angle annular-dark-field (HAADF) lattice images, acquired in a transmission electron microscope with the electron beam focused onto the sheet, are directly interpretable: bright contrast corresponds to atoms, whereas dark contrast corresponds to gaps in between atoms. Effects of atomic structure extending in the direction of the electron beam, resulting in dechanneling of the beam on atomic columns, and hence inducing contrast changes etc., cannot occur in monolayer structures. Any observed changes in the periodicity of the lattice image, in the absence of other discernible features (e.g. hydrocarbon contamination layers, phases containing impurities/different elements, or multiple graphene sheets), must arise from apparent changes in the projected bond length. Furthermore, when this occurs over regions comprising of many lattice units, it must arise from out-of-plane bending of the atomic bonds to form sheet undulations. The presence of defects can be confirmed by inspection of HAADF images; if present, they would only give rise to extremely localized and isolated changes. Elastic strain would be expected to result in bond stretching; however, as we will demonstrate later, in 'distorted' regions we observe a shortening of the bonds. Spatial periodicity changes are thus a direct manifestation of sheet 'crumpling'. Atomic resolution phase contrast bright-field (BF) images acquired from a monoelemental monolayer, under the same conditions as those used for HAADF imaging (i.e. at near focus and in the absence of 3D structures), provide the same information regarding out-of-plane bending as HAADF images. However, an advantage of BF imaging arises from the stronger contrast, which enables time-series acquisition, revealing changes in ripple patterns in subsequent images at reasonable exposure time. The disadvantage is that although phase contrast reveals periodicities, it is not a direct depiction of atomic positions, and hence requires careful interpretation.

Ursel Bangert's research has focussed on the advancement and exploration of electron microscopies/spectroscopies with ultra-high spatial resolution – applied, in particular, to nanostructures. Regarding materials' applications the current focus is on the controlled introduction of impurities into carbon nanotubes, semiconductor nanocrystals and graphene using ion beam methods, to help understand the microstucture–electronic structure relationship at the atomic level, i.e., the effects of individual impurity atoms on local bonding, defects and dielectric response. The ion beam modification aspect of nanostructures is specifically aimed at tailoring plasmons for plasmonics applications.

Mhairi Gass obtained her Ph.D. on scanning transmission electron microscopy (STEM) at Liverpool in 2004. After a short stint at Cambridge working on electron tomography she moved to the SuperSTEM facility where she has worked on high resolution imaging and spatially resolved energy loss spectroscopy, which has resulted in a number of high impact publications over a range of materials systems.

Andrew Bleloch did his Ph.D. at the Cavendish Laboratory, Cambridge. He was a leading member of the team that set up the Aberration Corrected Scanning Transmission Electron Microscipy Facility at Daresbury in the UK, known as SuperSTEM. He ran that facility from 2002 to 2008 and is now a Reader at Liverpool University with a more supervisory role as the Principal Investigator of the grant supporting the SuperSTEM facility. He is motivated by the need to characterise nano-materials atom-by-atom in order to engineer and understand these materials.

2 Experimental Large, freely suspended graphene membranes were produced by a combination of micromechanical cleavage, several steps of photolithography and electrodeposition. Using this method, membranes of 100 μm lateral extent and directly attached onto a TEM copper grid [10] were released. Proof that these indeed constituted single layers was based on their Raman and optical properties [11], as well as on their unique plasmon behavior [12], in conjunction with quantification of their contrast in HAADF images [13]. All data were acquired in an aberration-corrected scanning transmission electron microscope (STEM) [14] (the Daresbury SuperSTEM), operated at 100 kV. This microscope is well characterized for its scan distortions [15], and it was ascertained they do not affect the analyses conducted herein.

The collection semi-angle was 24 mrad, and angle of the HAADF detector annulus 70–210 mrad. The is probe size was 0.1 nm and the image scan between 5 s and 10 s.

3 Results and discussion Observing perpendicularly onto an undulating plane of atoms, the bond inclination will cause variations in the projected bondlength. For example, inclinations of ~5° from the horizontal flat sheet will give rise to a change in the projected C–C bond lengths of ~1%. Ripples possessing a wavelength of 5 nm, thus have an amplitude of 0.25 nm (this value being de-

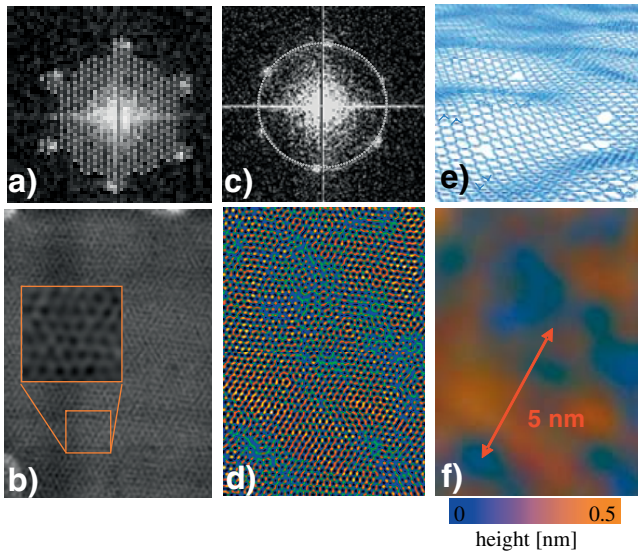

Figure 1 (online colour at: www.pss-a.com) a) A typical FFT of a single layer graphene image with superimposed mask used to obtain the IFFT of the HAADF image in (b). The inset in the HAADF image shows the magnified lattice structure of the orange framed area. c) A ring mask typically used to construct IFFTs as in (d). The image in (d) is the inverse FFT of the HAADF in (b). e) Model of graphene, with undulations and defects. f) Gaussian-blurred image with the atomic detail in (d) removed, to highlight larger scale structure (flanks of undulations appear blue, approximate height scale given underneath in colour with flank inflection points set at zero).

rived from electron beam diffraction [7]). However, such bond length changes are not easily observed in raw or even low-pass filtered HAADF lattice images, as seen using the filter detailed in Fig. 1a. As FFTs of nano-scale areas, like in our case, are embedded in significant noise, the error in positioning the diffraction spot maxima gives rise to a bond length error of ~±2% in BF images, and with slightly less in HAADF images. Applying a narrow annular band pass filter, with a band width corresponding to ~0.04 Å, i.e., imposing a narrow ring mask on the Fourier transform (FFT) of the raw images, passes spatial frequencies within ~2% of a selected frequency corresponding to a real space distance. The inverse transform (IFFT) reveals locations of atoms with such spacings, although with possible rotations, through intense lattice fringes. For graphene, the color coding is selected such that atoms possessing the correct bond length appear orange. Should the projected bond length change by as little as 2% owing to out-of plane bending of the atoms, the lattice periodicity will become less visible in the IFFT, and blurred patches will occur at such locations. Such regions appear blue. An example of this procedure is shown in Fig. 1. Figure 1a details the low band pass filter used to enhance atomic positions in the HAADF image in Fig. 1b. In Fig. 1c and d, respectively, ring filter and the resultant IFFT for the projected bond length visualization are shown. In the IFFT detailed in Fig. 1d, atomic scale detail can be seen as a fine raster superimposed on the colors. To better reveal the sheet rippling effect, the atomic detail has been removed by a Gaussian blurring function in the image in Fig. 1f. In the Gaussian filtered images again, orange (blue) regions correspond to areas of small (large) deviations from the graphitic *a*-plane distance of pristine and perfectly flat graphene sheets. Any spatial frequencies outside an annular mask diameter corresponding to the graphitic *a*-plane spacing, will possess significantly weaker intensity; the color-coded IFFT resulting from both, a smaller or larger band pass would therefore be expected to exhibit more bluish colors. Since undulations reduce the projected bond length, they become visible in IFFTs obtained with a narrow ring mask.

We have obtained IFFTs of a number graphene images, using a series of filter diameters in each case, with increments corresponding to 0.02 Å (such an increment would arise from an inclination of ~5°), and with the above bandwidth of 0.04 Å. Although the ring mask increment lies within the error of measurement, it is still possible to follow gradual changes in contrast. In such a series of IFFT images, the spacing range covers ±10% variation of the graphitic *a*-plane distance. In each IFFT image, a different projected lattice spacing is passed by the respective filter and comes 'into focus'; this is equivalent to observing the lattice in slices 'cut' through the crumpled 3D graphene sheet at different distances parallel to the flat sheet reference plane. In Fig. 2a and b, selected images from a series of IFFTs using ring mask diameter increments as described are detailed, the masks were applied to raw, single layer images, i.e. allowing spatial frequencies both below and above the first order diffraction spot distance to pass. Figure 2 (uppermost and middle rows) detail identical features imaged in BF and HAADF, with their associated IFFTs. BF IFFTs for the same band pass are very similar in their overall pattern to those of HAADF images, taking into account that the color scheme is slightly different in both cases. This lends credibility to the method being applied to HAADF images with weak intensities. The strongest intensity variations (orange to blue) can be observed in Fig. 2 columns iv–vii, where the *a*-plane frequency has filtered through, whilst deviations from this band pass result in images of overall lower contrast (bluish colors, columns ii, iii and viii). In row c, the same method is applied to a 5-layer graphene sample, (the number of graphene layers was determined using the procedures described in [12]). The breadth of images which exhibit the brown-orange colors (columns iv–vii) reflects the accuracy limit of the measurement; however, the radius of the ring filter used in column v (arrowed) corresponds most closely to the *a*-plane spacing. We note that pattern changes with band passes larger than the graphitic *a*-plane frequency (right of arrow, i.e. in columns vi and vii.) arise from a reduction in the bond length projection. For example, the circled locations mark contrast inversions, where the lattice at the flank of a ripple comes into focus, and then out of focus. In a simplistic picture, the peaks/troughs of ripples should be 'in focus' at the same band pass as the flat sheet, and the flanks

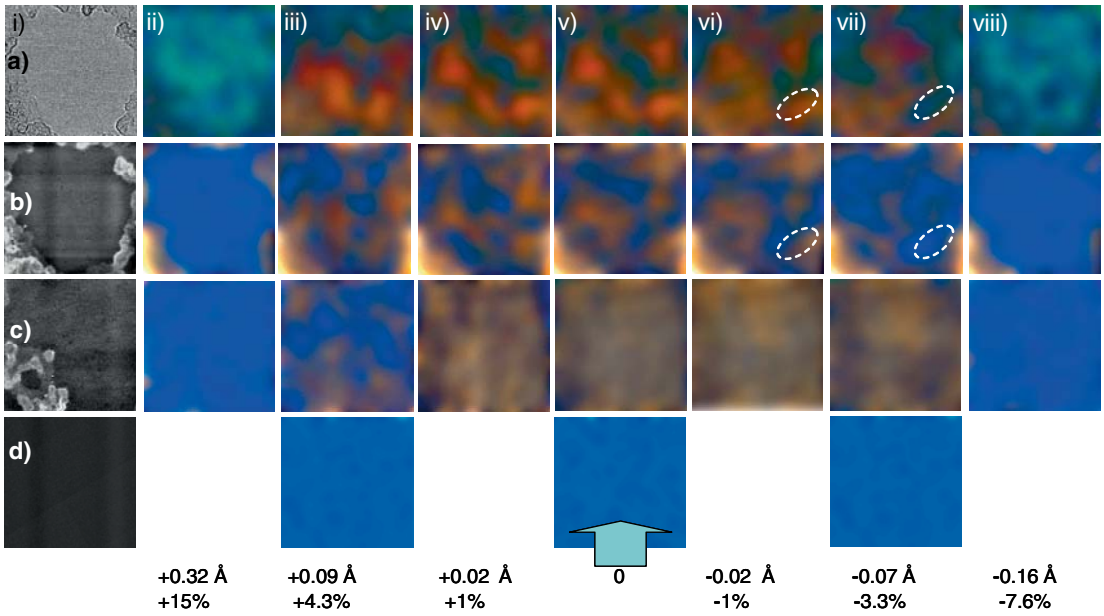

Figure 2 (online colour at: www.pss-a.com) a) Column (i) the BF lattice image of a single graphene sheet, from which the IFFTs in columns (ii) to (viii) are obtained. All IFFT images have undergone Gaussian blurring. The arrow in column (v) marks the image corresponding to the graphitic lattice spacing. Bandpass deviations from the graphitic *a*-plane spacing, and hence from the C–C bond length are, (ii) +15%, (iii) +4.3%, (iv) +1%, (v) none, (vi) –1%, (vii) +3.3% and (viii) –7.6%. b) Column (i) represents the HAADF lattice image of the same area as in (a). Columns (ii) to (viii) represent IFFTs of the image in (b) with the same band pass filters as above. c) Column (i) consists of the HAADF image of a 5-layer graphene patch. (d) An HAADF image and IFFTs of vacuum. The frame width of panels is 15 nm.

should then be 'out of focus'. The increment in the annular filter radius required to change the color from brown to blue (images in rows a and b, columns vi and vii, circled area), allows one to deduce the inclination angle as ~12°. The ripple width of ~5 nm yields a height of ~0.5 nm. Although this is slightly greater than the value reported [7, 8], ripples of this height are frequent in occurrence and pronounced in our samples. Ripples of lesser height are most likely present too, but they are concealed by larger undulations and are also close to the resolution limit of the present method: the smallest increment in Fig. 2 corresponds to 1% change in spatial frequency equivalent to ~6° inclination. The contrast variations reflect the complex and intricate sheet buckling, which is quite severe in certain regions.

Peng et al. [16] detail the introduction of various distortions in an aberration-corrected STEM, which is subsequently removed using an interpolation and shearing operation. In the present instrument the distortion has been well characterized; it is minimal and becomes manifest in a slight and systematical shift of the atoms along the vertical axis during the horizontal scan line duration. This distortion is negligible and therefore was not corrected. This is confirmed in the 'flat' contrast from the 5-layer graphene sample (Fig. 2c); it confirms furthermore that the observed contrast variations in single layers are not just due to the measurement procedure, e.g. statistical noise, electron beam fluctuations or artifacts from the FFT process. We have additionally applied this procedure to images acquired in vacuum (Fig. 2, row d). Here, the contrast is a slight small-scale patchiness, and the color, independent of the filter diameter, always remains blue.

Additionally, topography on a larger scale arising from thin hydrocarbon deposits, as can be seen bordering 'clean' areas, e.g. in the lattice image in Fig. 2a and b, also affects the IFFT image: such deposits introduce some amorphicity, hence many spatial frequencies are present in such locations, ranging from the lattice frequency down to low frequencies representing local, large scale disturbances. This accounts for the pink coloration occurring at such locations at all band passes.

Although undulations are observed in every clean graphene 'patch' (graphene area free from hydro-carbon deposit that is) in the absence of visible topological defects, we observe that the ripple patterns can, however, be influenced by the latter. For example in the HAADF image in Fig. 3a, a single vacancy can be observed in the uppermost right-hand quarter. A vacancy itself would appear as a point-like disturbance in the IFFT. However, the IFFT below shows deformation in an extensive area around it by the blue color, which relates to projected bond shortening of >5%. This cannot be C–C bond shortening, since strains of this amount cannot be maintained over such extended areas; hence the sheet must be bent. The ripple pattern appears to be the result of local changes in stiffness, which is reduced at vacancies and enhanced in regions with adatoms. The existence of the latter is deduced from HAADF images: Fig. 3a reveals variations in intensity at

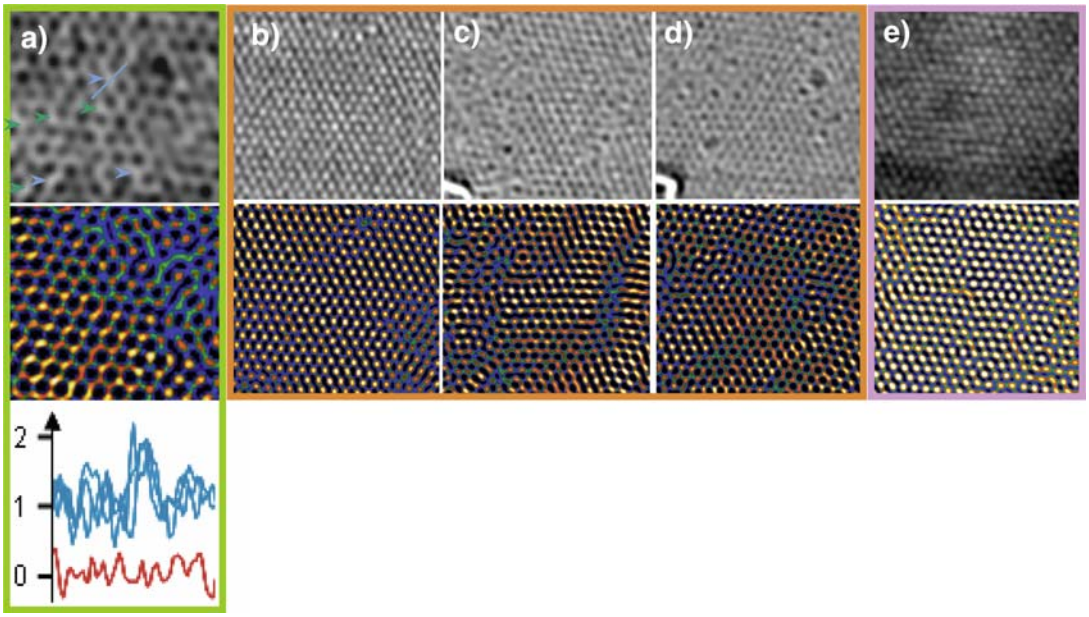

Figure 3 (online colour at: www.pss-a.com) a) HAADF lattice image and IFFT ripple image using the masks in Fig. 1a and b, respectively. The black region (in the uppermost right-hand quarter in the HAADF image) represents a vacancy and the brighter patches represent adatoms (arrowed). The blue lines are examples of intensity profiles acquired across brighter spots in the unfiltered image (blue arrows, the scan line is drawn in one case) and show ~2× the intensity of neighbouring C–C chains. The red curve is the vacuum intensity. Note the IFFT indicates bending around the vacancy, whereas the adatom region remains undeviated. The frame width is ~2 nm. b)–d) Same masks applied to high-resolution phase contrast STEM BF images of a time sequence (0th, 15th and 17th frame), with all images depicting precisely the same location. Vacancies introduced through e-beam irradiation are visible as dark dots in slightly underfocussed images, starting around the 15th repeat scan. Note the change in vacancy position in repeated scans (c) and (d). e) 5-layer graphene HAADF image and IFFT. The frame width in (b)–(e) is ~4 nm.

some of the C–C bonds. Intensity analysis (performed on *raw* HAADF images) has shown two levels of brightness within the atomic rings: patches of roughly twice the intensity occur frequently along C–C bonds. Some such locations are arrowed. Intensity profiles obtained at positions of blue arrows showing 'spikes' of twice the intensity are shown in the blue curves in Fig. 2a). Since Z-contrast scales nearly linearly with sample thickness, i.e. with the number of atoms (of the same species) encountered by the electron beam upon traversing the specimen, we can identify these brighter patches as positions of C-adatoms, forming bridges over in-plane C–C bonds [17, 18]. It appears vacancies lie in crinkles or at their flanks (the blue region in Fig. 3a), whilst regions of adatoms are generally flatter.

The defect distribution changes in each scan, indicating that vacancies heal/migrate easily under the electron beam. Accompanying this is significant modification in the appearance of the ripple pattern. This is demonstrated in the BF image, (Fig. 3b–d) representing the 0th, 15th and 17th image of a high-resolution phase contrast series obtained via repeated scanning of the same area. The BF image Fig. 3c shows the onset of increased vacancy formation. The time series was acquired in BF for the benefit of the shorter total acquisition time. The disadvantage is that unlike in HAADF images, Z-dependence is not revealed; hence chemical information such as the existence of adatoms cannot be disclosed. The IFFTs in Fig. 3 have not been blurred to enable correlation between lattice positions in both types of image. The ripple frequency is strongly related to the spacing of regions with vacancy accumulation. Figure 3e shows an HAADF STEM image of a 5-layer graphene specimen, along with its IFFT. The IFFT contrast is notably much more uniform (in spite of the fact that the HAADF image has a horizontal contrast step, presumably as a result of a change in tip emission) indicating that undulations, if present, have very much smaller amplitudes.

4 Conclusion In conclusion, in single graphene layers ripples of around 5 nm width (corresponding to a 10 nm undulation wavelength) are often present. This is not the case for few-layer graphene. The spatial modulation distance is in good agreement with recent numerical simulations [8], which demonstrate a distinct periodicity of ~8 nm for suspended graphene (given by the specifics of the C–C bond), and previous observations of ~15 nm ripples from convergent beam electron diffraction [9]). Meyer et al. [17] state that ripples are static, otherwise they would not be able to be discerned in an electron micrograph. However, we observe changes in the pattern over a time period of several seconds. Importantly, point defects (vacancies and adatoms) appear to significantly influence the stiffness of the graphene sheet. In particular, crumpling is

observed near vacancies, and the patterns modify with subsequent scans, as does the vacancy distribution. Hence rippling is facilitated by point defects; it does not represent permanent deformation, but rather dynamic flexing, aided by redistribution of the defects.

References

[1] D. R. Nelson, T. Piran, and S. Weinberg (eds.), Statistical Mechanics of Membranes and Surfaces (World Scientific, Singapore, 2004).
[2] D. R. Nelson and L. Peliti, J. Phys. (France) **48**, 1085 (1987).
[3] P. Le Doussal and L. Radzihovsky, Phys. Rev. Lett. **69**, 1209 (1992).
[4] K. S. Novoselov et al., Proc. Natl. Acad. Sci. USA **102**, 10451 (2005).
[5] K. S. Novoselov et al., Science **306**, 666 (2004).
[6] K. S. Novoselov et al., Nature **438**, 197 (2005).
[7] J. C. Meyer, A. K. Geim, M. I. Katsnelson, K. S. Novoselov, T. J. Booth, and S. Roth, Nature **446**, 60 (2007).
[8] A. Fasolino, J. H. Los, and M. I. Katsnelson, Nature Mater. **6**, 858 (2007).
[9] J. C. Meyer, A. K. Geim, M. I. Katsnelson, K. S. Novoselov, D. Obergfell, S. Roth, C. Girit, and A. Zettl, Solid State Commun. **143**, 101 (2007).
[10] T. J. Booth et al., Nano Lett. **8**, 2442 (2008).
[11] R. R. Nair, P. Blake, A. N. Grigorenko, K. S. Novoselov, T. J. Booth, T. Stauber, N. M. R. Peres, and A. K. Geim, Science **320**, 1308 (2008).
[12] T. Eberlein et al., Phys. Rev. B **77**, 233406 (2008).
In this paper, which presents results from the identical sample as in the present paper, we identify – with proof – areas of one, two, five and more graphene sheets via quantitative HAADF and plasmon spectroscopy in a STEM.
[13] M. H. Gass, U. Bangert, A. L. Bleloch, P. Wang, R. R. Nair, and A. K. Geim, Nature Nanotechnol. **3**, 676 (2008).
[14] O. L. Krivanek, N. Dellby, and A. R. Lupini, Ultramicroscopy **78**, 1 (1999).
[15] A. M. Sanchez, P. L. Galindo, S. Kret, M. Falke, R. Beanland, and P. J. Goodhew, J. Microsc. **221**, 1 (2006).
[16] Y. Peng, M. P. Oxley, A. R. Lupini, M. F. Chisholm, and S. J. Pennycook, Microsc. Microanal. **14**, 36 (2008).
[17] J. C. Meyer, C. O. Girit, M. F. Crommie, and A. Zettl, Nature **454**, 319 (2008).
[18] K. Nordlund, J. Keinonen, and T. Mattila, Phys. Rev. Lett. **77**, 699 (1996).

